

**Shilan Jin**

Department of Industrial & Systems Engineering,  
Texas A&M University,  
College Station, TX 77843  
e-mail: jin0541@tamu.edu

**Ashif Iqbal**

Department of Industrial & Systems Engineering,  
Texas A&M University,  
College Station, TX 77843  
e-mail: ashif\_22@tamu.edu

**Satish Bukapatnam**

Department of Industrial & Systems Engineering,  
Texas A&M University,  
College Station, TX 77843  
e-mail: satish@tamu.edu

**Andrew Gaynor**

Design Optimization Team, Weapons and  
Materials Research Directorate,  
Army Research Lab,  
Aberdeen Proving Ground,  
Adelphi, MD 21005  
e-mail: andrew.t.gaynor2.civ@mail.mil

**Yu Ding**

Department of Industrial & Systems Engineering,  
Texas A&M University,  
College Station, TX 77843  
e-mail: yuding@tamu.edu

# A Gaussian Process Model-Guided Surface Polishing Process in Additive Manufacturing

*Polishing of additively manufactured products is a multi-stage process, and a different combination of polishing pad and process parameters is employed at each stage. Pad change decisions and endpoint determination currently rely on practitioners' experience and subjective visual inspection of surface quality. An automated and objective decision process is more desired for delivering consistency and reducing variability. Toward that objective, a model-guided decision-making scheme is developed in this article for the polishing process of a titanium alloy workpiece. The model used is a series of Gaussian process models, each established for a polishing stage at which surface data are gathered. The series of Gaussian process models appear capable of capturing surface changes and variation over the polishing process, resulting in a decision protocol informed by the correlation characteristics over the sample surface. It is found that low correlations reveal the existence of extreme roughness that may be deemed surface defects. Making judicious use of the change pattern in surface correlation provides insights enabling timely actions. Physical polishing of titanium alloy samples and a simulation of this process are used together to demonstrate the merit of the proposed method. [DOI: 10.1115/1.4045334]*

*Keywords: correlation parameters, endpoint, Gaussian process, pad change, polishing process, additive manufacturing, modeling and simulation*

## 1 Introduction

Polishing plays a critical role in making additive manufacturing (AM) products practically useful. By the nature of AM, the surface of its products, without post-processing, are too rough to meet designed tolerances. For many metal AM products, surface polishing is inevitable [1]. Studies also show that polished surface finish significantly enhances the fatigue life of AM products [2].

In practice, polishing is carried out over multiple stages for creating a desired surface finish [3,4]. Pads of progressively decreasing grit sizes, oftentimes with increasing pad stiffness, are employed over these stages. Within each polishing stage, the asperities of particular sizes (scales) are removed as a result of repetitive relative motion between asperity and the polishing pad with fixed or loose abrasive grains [5]. Two decisions regarding pad operations agonize practitioners in part because they have to be tailored for each particular polishing process—(1) when to change the polishing pads and (2) when to stop the entire polishing process.

A pad change is warranted for two reasons. The first reason stems from pad deterioration, as the action of polishing understandably deteriorates the surface quality of a polishing pad. The second reason is to transition from the current grit to a finer grit. The key trigger for the pad change in this latter case is the cessation of asperities of particular scales being uniformly distributed over a workpiece surface. Consequently, no matter which reason it is, the use of a worn-out or ineffective polishing pad could harm the product surface under polishing, rather than improve it, a phenomenon known as over-polishing. While prior research has yielded approaches to automate the detection of pad damage (i.e., the first

reason) [6,7], a systematic approach to decide the end of a polishing stage based on cessation of a set of asperities (i.e., the second reason) has not been addressed in the literature.

The current practice for polishing process decision making relies heavily on practitioners' visual inspection of the surface roughness condition. That the polisher's intuition of when the surface condition plateaus out and when the pad damage sets in plays a critical role in deciding when to stop the polishing process. Consequently, significant process cycle time is consumed by repeated stoppage and surface inspections (visual or through the use of instruments) [8,9]. Quantitative surface roughness metrics do exist, and the most commonly used during polishing in industry is the average roughness parameter, denoted by  $Ra$  for one-dimensional profiles or  $Sa$  for two-dimensional areas [10]. The average roughness parameter is calculated, using surface measurements taken by a profilometer, as the mean absolute deviation (MAE) about the center line within the evaluation length or area. Recent advances in optical imaging and microscopy allow fast estimation of  $Sa$  over vast areas of an AM product [11]. Even so, in our research, we discover that while the surface roughness measure could be useful as an average indicator of the rough level of a surface, it does not adequately capture other subtleties of surface textures and may mislead the decision process.

Let us consider the simple examples in Fig. 1, in which the order of the  $Sa$  values contradicts the intuitive roughness of the respective surfaces. The three surfaces in Fig. 1 have their roughness values, respectively, as  $Sa = 0.036 \mu\text{m}$ ,  $Sa = 0.034 \mu\text{m}$ , and  $Sa = 0.028 \mu\text{m}$ . The surface in Fig. 1(a) is noticeably smoother than those in Figs. 1(b) and 1(c). Yet, the three  $Sa$  values are close to each other. Worse, the  $Sa$  value associated with Fig. 1(c) is even smaller than that associated with Fig. 1(a). Apparently, using  $Sa$  to select the best surface could be counterproductive. We will present in the later section more examples to show the limitation of the current surface roughness measure.

Manuscript received May 29, 2019; final manuscript received October 20, 2019; published online October 30, 2019. Assoc. Editor: Radu Pavel.

This work is in part a work of the U.S. Government. ASME disclaims all interest in the U.S. Government's contributions.

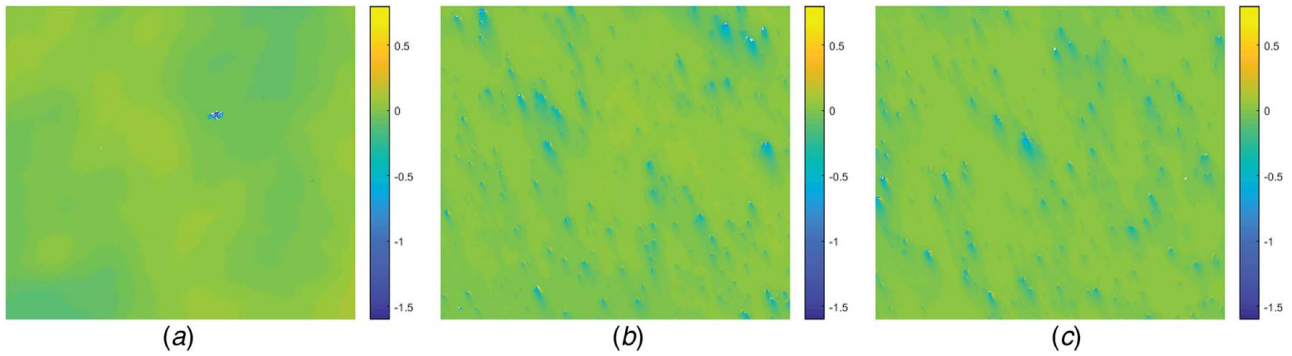


Fig. 1 Different surfaces but similar  $S_a$  values: (a)  $S_a = 0.036 \mu\text{m}$ , (b)  $S_a = 0.034 \mu\text{m}$ , and (c)  $S_a = 0.028 \mu\text{m}$

In our research, we explore and investigate the strategies and options of a model-guided decision process for the polishing of metal AM products. It does not come as a surprise that Gaussian process (GP) turns out to be a useful modeling tool for this purpose. GP modeling is widely used in spatial statistics [12] and later extended for broader purposes of machine learning [13]. If we treat the measurements taken by a profilometer at multiple locations on a product surface as if they were spatial measurements taken over a landscape, then the relevance of GP becomes self-evident. We discover that the correlation parameters associated with polishing stages can reveal the subtle features of the surface as well as their changes during the polishing process. Making judicious use of this insight leads us to devise a GP model-guided decision protocol for advising important actions in the polishing processes.

We understand that GP models have been used in the AM applications but want to stress that their current and previous uses are for different purposes. Moroni et al. employ a GP model to estimate the deviation of a real rough surface from the computer-modeling nominal smooth surface to give the designer a more accurate preview of the additive manufactured parts [14]. Tapia et al. develop a GP regression model to predict the part pore generation during a selective laser melting process and to express the porosity with respect to certain processing parameters, such as laser power, scanning speed, and layer thickness [15]. Tapia et al. build a generic workflow process based on GP regression to understand the uncertainty in the laser powder-bed fusion process [16]. To our best knowledge, we are the very first to develop a GP model to guide the decision making in a polishing process of metal AM products.

The rest of the paper unfolds as follows. Section 2 describes the data collection process and provides a  $S_a$ -based preliminary analysis of the surface roughness. Section 3 presents the GP model devised to reflect the dissimilarity among local areas of the surface, in order to capture subtle surface features and their changes over time. The GP model-guided decision rule is then proposed for informing pad change and the endpoint. Section 4 analyzes the data from two physical polishing experiments, while Sec. 5 analyzes the data from a simulated polishing process, together these case studies demonstrate the merit of the proposed method. Section 6 summarizes our work with some concluding remarks.

## 2 Polishing Experiment Data and Preliminary Analysis

In this research, we focus on the polishing process of a metal AM product and, specifically, the 3D-printed Ti-6Al-4V alloy samples. The printing process to obtain these samples involves depositing a  $50 \mu\text{m}$  layer of Ti-6Al-4V powder that consists of Ti-6Al-4V particles of average diameter of  $72 \mu\text{m}$  using a focused beam of 3 mA and a scanning speed of 10 m/s [17]. Each of the Ti-6Al-4V alloy samples is polished from a raw stage (Fig. 2(a)) to a smooth stage (Fig. 2(e)) with a specular surface finish. Figures 2(b) through 2(d) show the surfaces at intermediate stages during the polishing process.

During the polishing process, we pause the polishing action from time to time and take surface measurements using a ZeGage™ 3D optical profiler, named “Zygo” after its producer. The polishing process is therefore discretized at the pausing times, each of which is referred to as a “stage” and denoted by  $t \in \{1, \dots, T\}$ , where  $T$  is the total number of stages.

At each stage, a total of  $M$  inspection locations are randomly sampled over the surface of the Ti-6Al-4V alloy sample. Zygo is used to take measurements at each of the  $M$  locations. The Zygo measurements are not a single scalar output but a profile image covering a small local area of  $800 \times 800 \mu\text{m}^2$ . The  $800 \times 800 \mu\text{m}^2$  area is divided into  $1024 \times 1024$  pixels, and Zygo measures the surface height at each pixel. One can conceptualize the surface measurements as a collection of  $M$  height matrices, each of which is of  $1024 \times 1024$  dimensions. Please see the illustration in Fig. 3.

We use  $\mathbf{x} = (x_1, x_2)$  to denote the coordinate of a location and use  $X, Y$  to denote the index of pixels within a location, such that  $X \in \{1, \dots, 1024\}$  and  $Y \in \{1, \dots, 1024\}$ . The pixel height is denoted by  $z$ . In Zygo measurements,  $z$  can be either positive or negative. We refer to a positive height as a peak and a negative height as a valley.

Within each location, the local surface roughness is characterized by the three-dimensional data set  $\{(X, Y, z)\}$ . But handling a 3D dataset can be burdensome. Following what is proposed by Stewart [18], we choose to convert the 3D response surface to a 2D profile, known as the bearing area curve. The bearing area curve is basically a quantile curve, i.e., ordering the  $z$  values associated with the pixels from the largest to the smallest and plot them

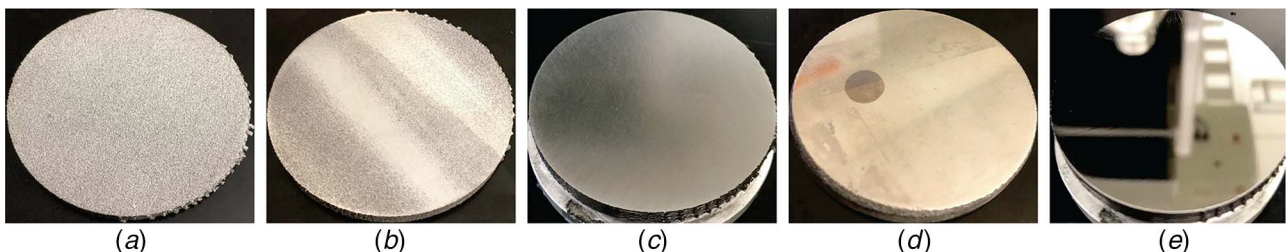
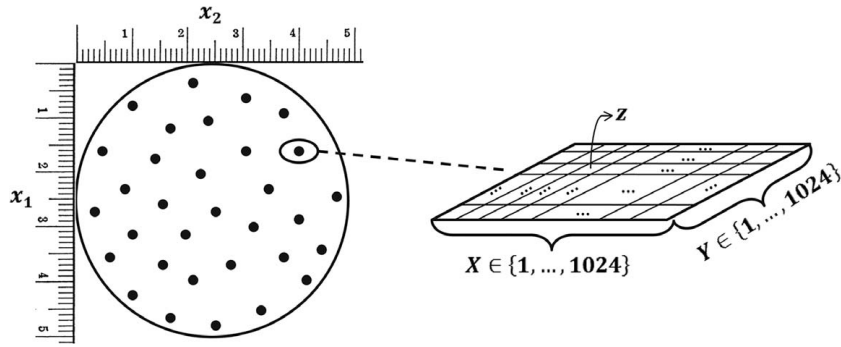


Fig. 2 Illustration of surface roughness of the Ti-6Al-4V sample along the polishing process



**Fig. 3** An illustration of  $M$  inspection locations and the magnified view within an inspection location

against the quantile values. Figure 4(a) presents an example of the quantile curves at one of the polishing stages. For the  $M$  locations on the sample at stage  $t$ , the surface measurements manifest as the collection of  $M$  quantile curves, as shown in Fig. 4(b).

Based on the surface measurements at each location,  $Sa$  can be calculated for that location as follows:

$$Sa = \frac{1}{1024 \times 1024} \sum_{X=1}^{1024} \sum_{Y=1}^{1024} |z_{X,Y} - \bar{z}| \quad (1)$$

where  $\bar{z}$  is the sample average of all  $z$ 's associated with the same location. Over the whole surface, there are  $M$  distinct  $Sa$  values. Understandably, the  $Sa$  values are different at different locations. The variation and distribution of  $Sa$ 's can be visualized using a boxplot per stage.

On one of the Ti-6Al-4V alloy samples, we take surface measurements at a total of 22 stages, i.e.,  $T=22$ . At each stage, the number of locations is  $M=32$ . We plot the boxplots of  $Sa$ 's over the 22 stages, as in Fig. 5(a), where the horizontal bar in a box indicates the median of  $Sa$ 's for that stage. It is not difficult to notice that the median of  $Sa$ 's sees a sharp decline in the very early stages but soon plateaus. Figures 5(b) and 5(c) present the  $Sa$  boxplots for a range of stages so that the boxplots are not too much compressed due to too large a value at the early stages.

The use of median  $Sa$  certainly does not inform when to change the polishing pads. It is difficult to signal when to stop, too. If one stops after the initial rapid descent, say, at stage 3 or 4, doing that

would be surely premature. If not, when else is a good time to stop? After the initial descent, the fluctuation in  $Sa$  certainly frustrates practitioners.

In addition to the lack of clear clues informing decisions in the polishing process, we also observe that the median  $Sa$  value at stage 10 is smaller than that at stage 11. Let  $\overline{Sa}_t$  denote the median of  $Sa$ 's at stage  $t$ . Then,  $\overline{Sa}_{10} = 0.069 \mu\text{m}$  and  $\overline{Sa}_{11} = 0.123 \mu\text{m}$ . On surface, this may leave an impression that the surface quality gets worse from stage 10 to stage 11, meaning that the polishing action in between is harmful rather than helpful. But a closer look indicates that the opposite is true. At stage 10, although the overall surface is reasonably flat (Fig. 6(a)), there exist multiple, isolated surface anomalies like spikes or scratches (Fig. 6(b)). The polishing process from stage 10 to stage 11 in fact removes many of these surface anomalies and indeed improves the surface quality. Such subtle surface features are not captured by the median  $Sa$  values. The limitation of the current decision metrics calls for new modeling and decision rule development.

### 3 Gaussian Process Model for Polishing Decisions

The inconsistent human's intuition and unsatisfactory  $\overline{Sa}$  representation raise the need of developing a model-guided polishing decision process. Our goal is to find out a simple quantitative measure that can reflect the surface subtleties, complementing  $Sa$  that represents the average roughness. Based on these two

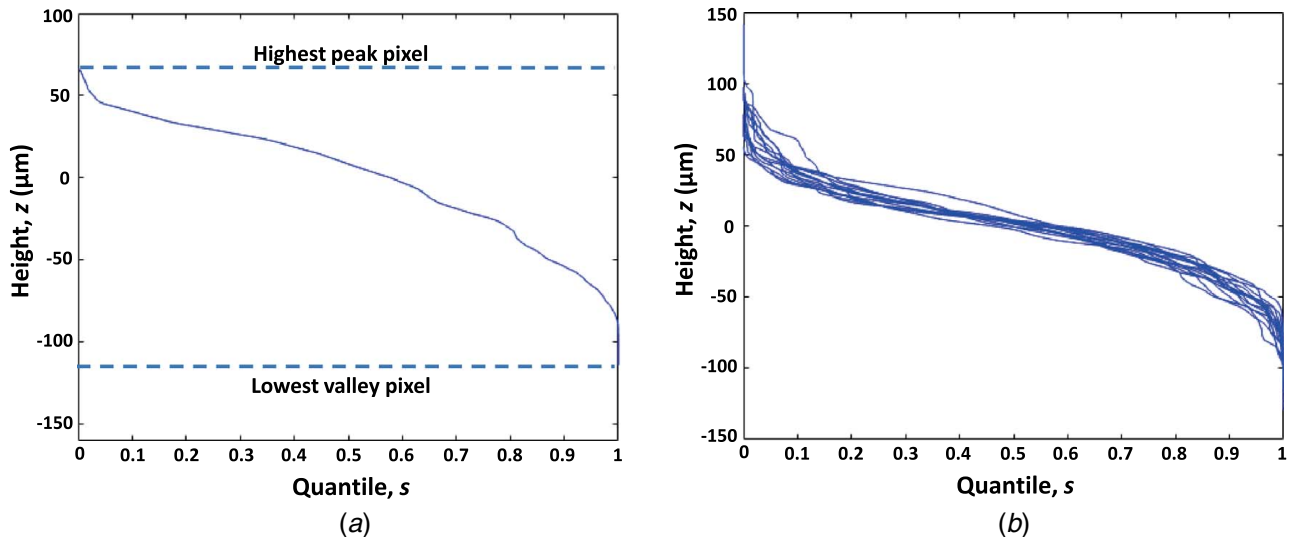


**Fig. 4** Illustration of quantile curves: (a) quantile curve of one inspection location and (b) quantile curves of all  $M$  locations on the sample surface

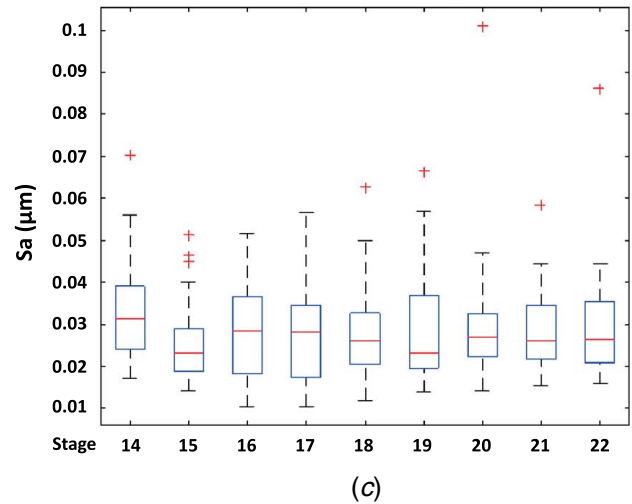
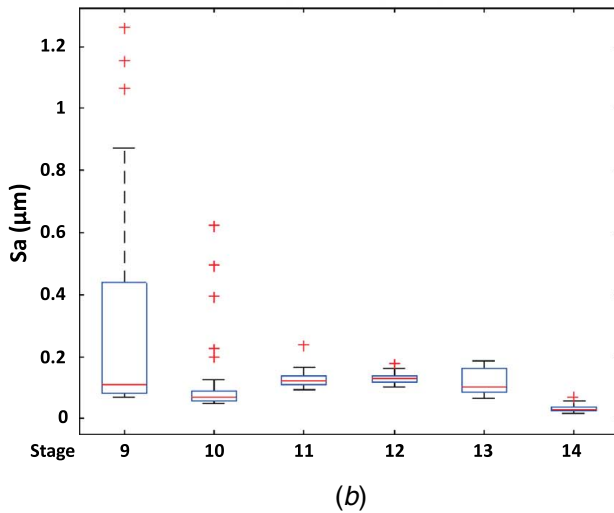
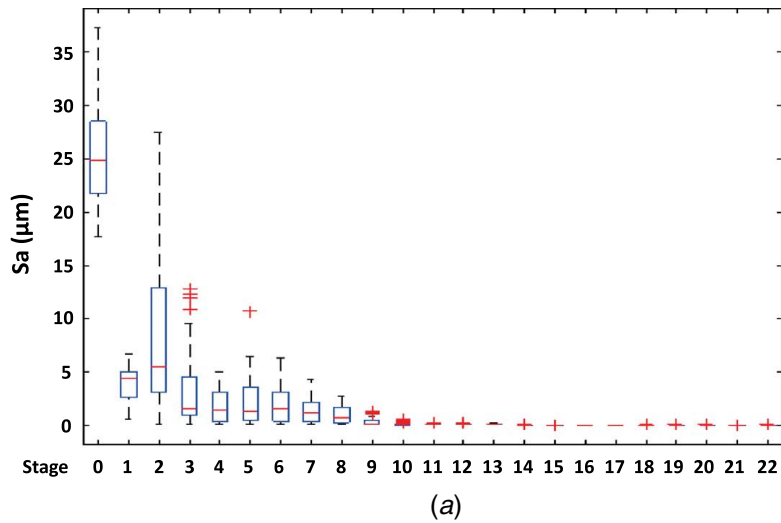


**Fig. 5 Overview of the Sa boxplots during the polishing process: (a) Sa boxplots for all stages, (b) Sa boxplots from stages 9 to 14, and (c) Sa boxplots from stages 14 to 22**

measures, a polishing operation decision rule is then developed to accommodate the need for online measurement and operation of polishing processes.

**3.1 Modeling of the Surface Roughness Data.** We model the responses at each stage individually and then use the estimated model parameters to draw inference about the status of the polishing process.

For a given stage  $t$ , the surface roughness data are expressed in a collection of  $M$  quantile curves, each associated with one inspection location. Denote by  $s$  the horizontal axis of the quantile curve plots in Fig. 4. Recall that the vertical axis is denoted by  $z$ . Counting the location coordinates,  $(x_1, x_2)$ , there are three inputs, which we use  $\mathbf{w}$  to denote, namely,  $\mathbf{w} = (s, x_1, x_2)^T$ .

We devise the following GP model for stage  $t$ :

$$z^t(\mathbf{w}) = \beta_0^t + \tau^t(\mathbf{w}) + \epsilon^t, \quad t = 1, \dots, T \quad (2)$$

where the superscript “ $t$ ” signifies the stage dependence. In the above model, we simplify the general mean trend function by a constant  $\beta_0$ . This is a common treatment in GP modeling [13], because a GP model is nonparametric in nature and rather flexible to model a wide variety of nonlinear response surfaces so that a nonlinear mean function may not be necessary. The second term,  $\tau^t(\mathbf{w})$ , is the stochastic term of a multivariate Gaussian distribution,  $\mathcal{N}(\mathbf{0}, \mathbf{K})$ , where the covariance matrix  $\mathbf{K}$  is to be modeled

through a covariance structure as discussed in the sequel. The stochastic term,  $\tau^t(\mathbf{w})$ , is to capture systematic features over the polished surface at both scales: the micro-scale within a location associated with  $s$  and the macro-scale between locations associated with  $(x_1, x_2)$ . Rasmussen and Williams [13] analyze how the smoothness of the sample path curve is affected by the correlation parameters. In our GP model, the smoothness of the response at a single location is represented by the micro-scale correlation parameter, while the similarity among the response curves is characterized by the macro-scale parameters. The more dissimilar among the adjacent locations over the surface, the more evident that further polishing is needed for the surface. The last term,  $\epsilon^t$ , is the independently and identically distributed (i.e., i.i.d.) random noise of a zero mean and a stage-dependent variance,  $(\sigma_c^t)^2$ . Often the superscript  $t$  is dropped, e.g., the variance is expressed as  $\sigma_c^2$ , when there is no danger of ambiguity.

The original surface roughness data at any given stage is a set of functional responses. A number of past research efforts choose to model and solve such a problem via a functional GP model [19–21]. Our treatment is a little different. By discretizing the variable  $s$ , the GP model in (2) can be solved in a regular GP modeling fashion. This simplifies the modeling and solution procedure and we believe doing so facilitates the use of the model in engineering applications. To guide the choice in discretization, a sensitivity analysis is conducted in Sec. 4.1, Fig. 7, for selecting the proper sample size.

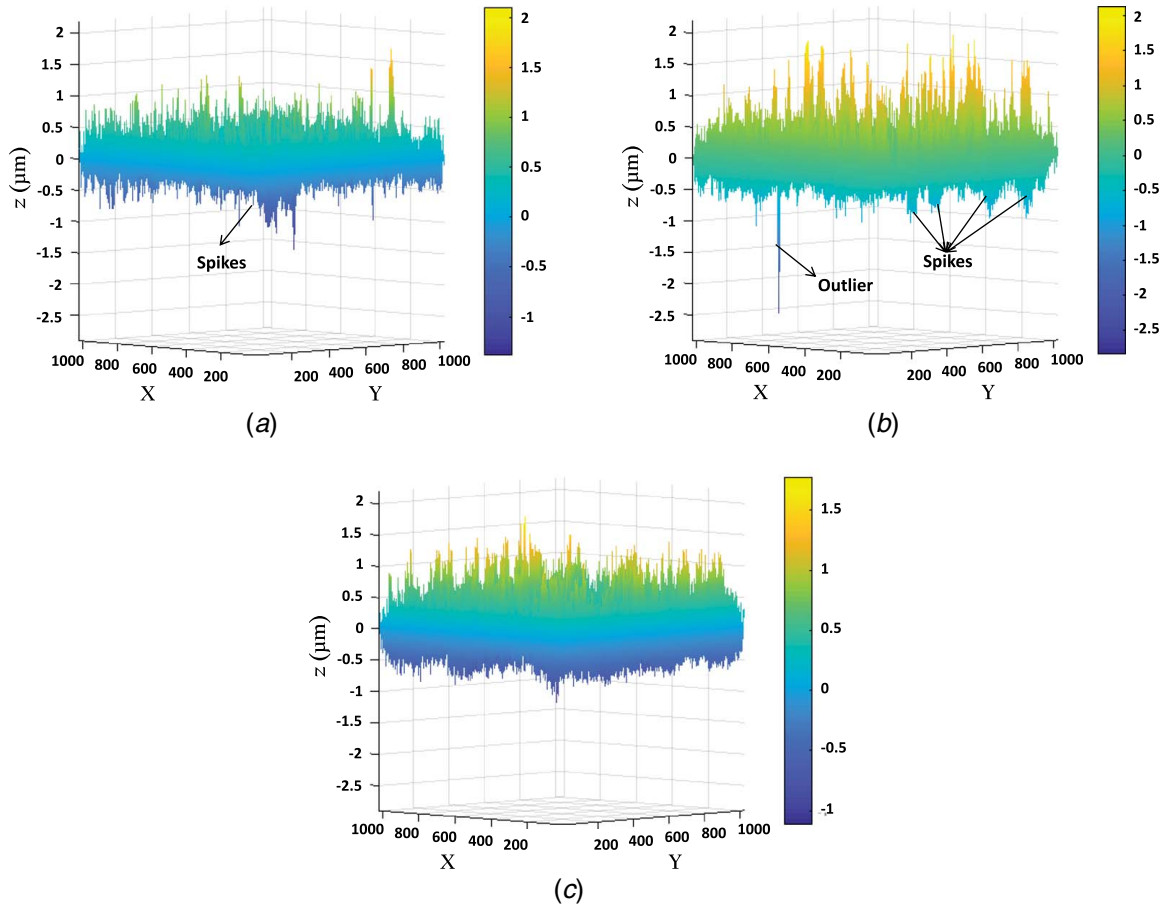


**Fig. 6 Median  $S_a$  misses anomalies in surface roughness: (a) the local surface averaged over all  $M$  locations at stage 10, (b) surface anomalies at certain location at stage 10, and (c) the local surfaces at stage 11: slightly increased roughness but almost no spikes**

A key issue in GP modeling is to specify the covariance function for the stochastic term,  $\tau'(\mathbf{w})$ . We use a squared-exponential covariance function, arguably the most commonly used one in GP modeling [13], as follows:

$$k(\mathbf{w}, \mathbf{w}') = \sigma_\tau^2 \cdot \exp \left\{ -\frac{1}{2} \left( \frac{\|\mathbf{x} - \mathbf{x}'\|^2}{\theta_x^2} + \frac{|s - s'|^2}{\theta_s^2} \right) \right\} \quad (3)$$

Here, we assume that the Gaussian random field over the polishing surface is isotropic so that there is one common scale parameter,  $\theta_x$ , used for both  $x_1$  and  $x_2$  directions. The scale parameter for the quantile curve is different, which is denoted by  $\theta_s$ . We believe that the assumption of isotropy over the polishing surface is reasonable, because the AM part is subject to quasi-random orbital motion as the polishing process progresses. There is no evidence to suggest that the surface roughness along one direction differs substantially from that along another direction. In (3), all terms are stage dependent, but for notational simplicity, the stage superscript  $t$  is not shown explicitly.

Once the covariance function,  $k$ , is specified, it can be used to compute the covariance matrix. Along the  $s$  axis of a quantile curve, there are 1, 048, 576 pixels. To make the computation easier, we sample a subset of  $S$  pixels with their quantile values and respective roughness heights. In the experiments, this  $S$  is usually kept less than 100, which is numerous enough to represent a quantile curve. The total number of data points used for this GP model is then  $N = M \times S$ . The covariance matrix for the  $N$  data pairs,  $(\mathbf{w}_i, z_i)$ ,  $i = 1, \dots, N$ , is denoted by  $\mathbf{K}_{NN}$ , whose  $(i, j)$ th element,  $(\mathbf{K}_{NN})_{i,j}$ , is simply  $k(\mathbf{w}_i, \mathbf{w}_j)$ .

Under such a model set up, the parameters to be estimated for the GP model at stage  $t$  are  $\Theta^t = \{\beta_0^t, \sigma_\epsilon^t, \theta_x^t, \theta_s^t, \sigma_\tau^t\}$ . These parameters can be estimated for a specific stage by maximizing the log-likelihood function in (4):

$$\log p(z|\Theta) = -\frac{1}{2} (z - \beta_0)^T [\sigma_\epsilon^2 \cdot \mathbf{I} + \mathbf{K}_{NN}]^{-1} (z - \beta_0) - \frac{1}{2} \log |\sigma_\epsilon^2 \cdot \mathbf{I} + \mathbf{K}_{NN}| - \frac{N}{2} \log (2\pi) \quad (4)$$

where the stage subscript  $t$  is omitted for notational simplicity.

**3.2 The Gaussian Process-Based Decision Rule.** The scale parameters of the GP model in (2) reflect the strength or weakness of spatial correlation. Understandably,  $\theta_x$  reveals the correlation among different locations, whereas  $\theta_s$  is corresponding to the smoothness of the quantile curve. As we are more concerned with the polishing quality over the whole sample surface,  $\theta_x$  is of a greater value to our decision process. The scale parameter,  $\theta_s$ , may be used as a secondary indicator for the purpose of model representation verification. In our physical experiments, we found that for the time being, using  $\theta_x$  without consulting  $\theta_s$  appears to be sufficient.

In the initial stages, the workpiece consists of undulations and defects. Existence of these aberrations increases the spatial heterogeneity across the sample, resulting in a smaller  $\theta_x$  (i.e., low spatial correlation). As the polishing progresses, the sample surface gradually becomes smoother, thereby increasing the spatial correlations as well as the value of  $\theta_x$ . However, due to the presence of noise,

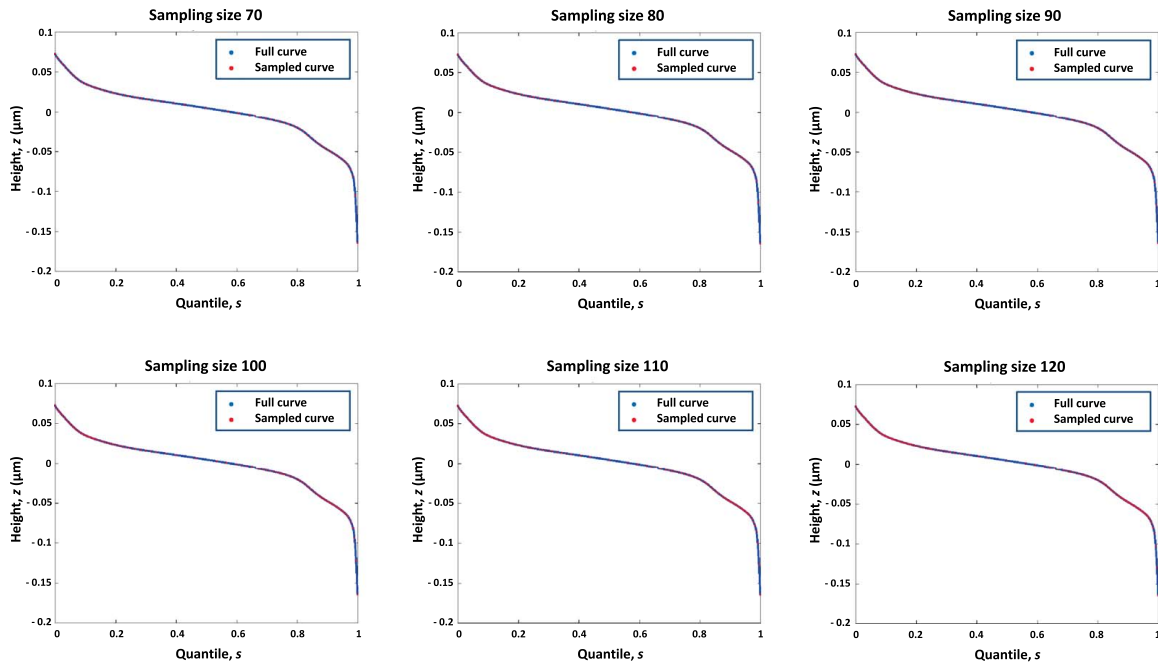


Fig. 7 Sensitivity in the number of pixels used to sample the quantile curve

a number of complexities must be accounted for in the decision process and they are elaborated in the following.

First, the overall roughness of the surface is decreasing, resulting in a stage-varying reference level for quantifying  $\theta_x$ . This means that what value of  $\theta_x$  is considered large and what is small is not absolute but relative. Second,  $\theta_x$  does not increase monotonically. Rather, it could decrease at some stage. Recall the over-polishing phenomenon discussed earlier. At certain point, due to the deterioration or ineffectiveness of the polishing pad, a continuing polishing could introduce pits and scratches (shown as spikes in Fig. 6) to an otherwise smooth surface. Over-polishing explains to certain extent the fluctuation in  $\bar{S}a$  as well as in  $\theta_x$ . Our analysis shows that  $\theta_x$  is more sensitive and hence a better indicator.

With these thoughts in mind, when devising a decision rule, it is a robust practice if we track and check the trend in the change of  $\theta_x$ , rather than compare it with an absolute threshold. Moreover, recall that the pad change is usually warranted for two causes. To distinguish the cause of pad deterioration from the need of grit size transition, we include an average indicator of the surface quality that pads of a specific grit size can achieve. We do not intend to introduce unnecessary measurement actions. Practically, the median  $Sa$  value as a loose threshold for distinguishing the causes is sensible. In the end, the scale parameter,  $\theta_x$ , and the median  $Sa$  are used together to advise decision making in the polishing process, i.e., the rule is that the surface of a high  $\theta_x$  and with a median  $Sa$  above the loose threshold is considered for the need of refreshing a pad of the same grit size, while a high  $\theta_x$  and a median  $Sa$  below the threshold is time for changing the pad. Both quantities, the median  $Sa$  and  $\theta_x$ , are available from the surface measurements taken at each stage.

The last consideration is the introduction of an initial phase in which we do not invoke the use of the GP model parameters. We discover that until the initial, rough morphology of the asperities is polished off, there is not much a trend in  $\theta_x$ , and using it does not add much value to the decision-making process. Clearly, no experienced engineer would stop in the early polishing stages anyway. Therefore, our use of the GP model skips the initial phase, which is determined based on a prescribed median  $Sa$  threshold. The following Algorithm 1 presents the decision-making process for pad change and polishing endpoint, as advised by the GP model.

In algorithm 1,  $\alpha$  is a constant, introduced to signal a change in  $\theta_x$ . Because  $\theta_x$  is estimated from noisy data, it is naturally subject to

variation. Using a constant thresholding, e.g.,  $\alpha=0.9$  or  $0.95$ , is a simple but effective way to avoid being overly sensitive to changes in the parameters. Too large a value of  $\alpha$  (close to 1) may result in frequent pad changes, while too small a value may miss detecting timely the formation of additional scratches and defects. We recommend using  $\alpha=0.9$  and setting that as the default value. We tested the use of  $\alpha=0.95$  and found it will not make much difference in our application. We want to note that using 90–95% of the peak value, rather than the peak value itself, is a rather common engineering practice to combat the adversary impact of noise and disturbance. As for the median  $Sa$  threshold, we recommend it to be around  $0.5 \mu\text{m}$  for the best result of a 800-grit pad (of abrasive size  $13 \mu\text{m}$ ), around  $0.2 \mu\text{m}$  for a 1200-grit one (of abrasive size  $8 \mu\text{m}$ ), and around  $0.05 \mu\text{m}$  for a fine polishing microcloth (with the use of alumina of abrasive size  $0.6 \mu\text{m}$  suspended in an aqueous solution).

**Algorithm 1** GP model-guided decision rule for pad change and endpoint

- (1) Initialize  $t-1 \leftarrow 0$  and  $\theta_x^{(t-1)} \leftarrow 0$ .
- (2) If  $\theta_x^{(t)} < \alpha \cdot \theta_x^{(t-1)}$ , go to step 3; otherwise, go to step 4.
- (3) If  $\bar{S}a$  is greater than the pre-specified  $\bar{S}a$  threshold, clean the current pad or use a new pad but of the same grit size; otherwise, change to a pad of finer grit size.
- (4) Set  $t-1 \leftarrow t$  and  $\theta_x^{(t-1)} \leftarrow \theta_x^{(t)}$  and keep polishing to the next stage, Stage  $t$ . Repeat steps 2 and 3, until no finer pad is available when being suggested for a pad change in step 3.

## 4 Physical Polishing Experiments

To illustrate the use of Algorithm 1 in polishing processes, we conduct a Ti-6Al-4V sample polishing experiment, polishing it from a raw stage to a smooth stage. The polishing stages are shown in Fig. 10 in Appendix. A second polishing experiment using another raw Ti-6Al-4V sample is conducted based on polisher's experiences only to contrast the effectiveness with and without the guidelines of Algorithm 1. Besides, the data preprocessing procedures are imposed at each polishing stage to accommodate the accuracy and computational requirement for modeling.

**4.1 Data Preprocessing.** One data preprocessing action undertaken is to remove outliers that may be due to measurement errors and anomalies. The specific action is to rank in a boxplot the pixel heights, i.e., the  $z$  values, for a specific location and at a specific stage. Then, remove outliers flagged as the observations outside the two whiskers of the boxplot. The use of a boxplot is rooted in solid statistical footing and avoids using a fixed percentage for outlier removal. Our experience shows that doing so produces results more consistent and robust.

Recall that we sample a subset of pixels along the  $s$  axis to represent the quantile curves. To ensure the quality of sample representation of the curves, pixels are selected more densely in the tails of the curves than in the middle part of the curves. Our choice of the sample size is  $S=70$ . To investigate whether a larger subset is needed, we conduct a sensitivity analysis using  $S$  from 70 to 120. Figure 7 presents the curve fitting using different number of pixel samples. We do not see much additional benefit resulting from sampling a greater number of pixels.

**4.2 Polishing Guided by Algorithm 1.** In the first experiment reported here, we follow the general guideline for pad change and stopping as outlined in Algorithm 1. The experiment comprises a total of 26 stages, where stage 0 indicates measurements taken before any polishing action. We have at our disposal three grit sizes of polishing pad, which are, from coarsest to finest, the 800-grit, 1200-grit, and microcloth. The polishing process setting is shown in Table 1. The images of the AM part for all the 25 stages (excluding stage 0) are included in Appendix.

We conduct the modeling and parameter estimation at each stage. The resulting GP model parameters are listed in Table 2. In the last column of the table, we also include the median  $Sa$  values.

Among the GP model parameters,  $\beta_0$  indicates the offset of the reference plane from zero. For most of the stages, its values are close to zero. This means that the Zygo machine has a good self-calibration mechanism to locate the reference plane. The standard deviation of the noise,  $\sigma_e$ , declines rapidly and then plateaus at a small magnitude from stage 5 and onward. The standard deviation of the stochastic term,  $\sigma_\tau$ , trend-wise mirrors that of  $\overline{Sa}$ . This makes

sense because  $\overline{Sa}$  is the MAE of the surface, whereas  $\sigma_\tau$  is the standard deviation associated with the variability between locations. The MAE and standard deviation are not of the same values but they are related. The two scale parameters,  $\theta_x$  and  $\theta_s$ , are associated with between-location (macro-scale) and within-location (micro-scale) correlations. As discussed earlier, we primarily rely on  $\theta_x$  for decision making.

Our polishing process goes through the following phases, as advised by Algorithm 1:

- (1) *The initial phase.* Up to stage 4, it is the initial phase. Stage 4 is included in the initial phase because before completing that stage, one will not know for sure that  $\overline{Sa}$  is below the threshold of  $0.5 \mu\text{m}$ . Looking at Table 2, this breaking point makes sense if examining the values of  $\sigma_e$ , because after stage 5,  $\sigma_e$  plateaus at a much smaller magnitude. During this phase, there is no pad change nor expectation to stop the process occurring.
- (2) *The first pad change.* Following the decision rule in Algorithm 1, from stage 5 onward, we track the change in  $\theta_x$  and are keen to detect the first substantial decrease in it, which indicates likely occurrence of over-polishing. The specific rule used is  $\theta_x^{(i)} < \alpha \cdot \theta_x^{(i-1)}$ , where  $\alpha=0.9$ . The stage where the rule is triggered is stage 11, at which point we switch to the 1200-grit pad.
- (3) *The second pad change.* After the first pad change and following the same logic, we should have changed the pad again at stage 18 when more than 10% decrease in  $\theta_x$  is detected. Here, we purposely delay the pad change. We would like to observe what if we do not change the pad—Will the current pad continue to improve the surface or not? The 1200-grit pad is used from stage 19 through stage 22. By observing  $\overline{Sa}$  and inspecting the sample surfaces, we do not find much improvement by the extra steps of polishing using the same pad. The four extra steps take a total of 390 min. Should the original decision rule be followed, this much time would have been saved.
- (4) *The end point.* At stage 22, the polishing is switched to using a microcloth. With that, a change point is detected at stage

**Table 1 The physical polishing process settings for experiment #1**

From	To	Time (min)	Down force (lbs)	Head speed (rpm)	Base speed (rpm)	Pad	Alumina solution
Stage 0	Stage 1	5	10	100	50	800	No
Stage 1	Stage 2	5	10	100	50	800	No
Stage 2	Stage 3	10	10	100	50	800	No
Stage 3	Stage 4	10	10	100	50	800	No
Stage 4	Stage 5	10	10	100	50	800	No
Stage 5	Stage 6	15	10	100	50	800	No
Stage 6	Stage 7	15	10	100	50	800	No
Stage 7	Stage 8	15	10	100	50	800	No
Stage 8	Stage 9	15	10	100	50	800	No
Stage 9	Stage 10	15	10	100	50	800	No
Stage 10	Stage 11	15	10	100	50	800	No
Stage 11	Stage 12	15	10	100	50	1200	No
Stage 12	Stage 13	30	10	100	50	1200	No
Stage 13	Stage 14	30	10	100	50	1200	No
Stage 14	Stage 15	30	10	100	50	1200	No
Stage 15	Stage 16	30	10	100	50	1200	No
Stage 16	Stage 17	30	10	100	50	1200	No
Stage 17	Stage 18	70	10	100	50	1200	No
Stage 18	Stage 19	60	10	100	50	1200	No
Stage 19	Stage 20	60	10	100	50	1200	No
Stage 20	Stage 21	120	10	100	50	1200	No
Stage 21	Stage 22	150	5	100	50	1200	No
Stage 22	Stage 23	120	5	100	50	Microcloth	Yes
Stage 23	Stage 24	60	2	100	50	Microcloth	Yes
Stage 24	Stage 25	60	1	100	50	Microcloth	Yes

**Table 2 GP parameter estimates for experiment #1**

Stage	$\sigma_\epsilon$	$\theta_x$	$\theta_s$	$\sigma_\tau$	$\beta_0$	$\bar{S}_a$
Stage 0	0.2898	0.1141	0.0721	18.4327	-0.1886	25.924
Stage 1	0.0322	0.1316	0.0815	6.9842	-2.5420	11.405
Stage 2	0.0189	0.1215	0.0715	6.1934	-2.1364	6.510
Stage 3	0.0035	0.1026	0.0415	0.9928	-0.1037	1.398
Stage 4	0.0020	0.0820	0.0589	0.5251	-0.1310	0.304
Stage 5	$9.09 \times 10^{-5}$	0.0666	0.0692	0.4426	0.0031	0.118
Stage 6	$6.54 \times 10^{-5}$	0.0944	0.2972	1.4925	-0.2676	0.153
Stage 7	$5.28 \times 10^{-5}$	0.2051	0.1814	0.1790	-0.0220	0.135
Stage 8	$5.64 \times 10^{-5}$	0.2387	0.2266	0.4340	0.0790	0.144
Stage 9	$6.46 \times 10^{-5}$	0.2189	0.1900	0.3116	0.0376	0.163
Stage 10	$5.65 \times 10^{-5}$	0.2170	0.2126	0.3076	0.0392	0.141
Stage 11	$7.59 \times 10^{-5}$	0.1720	0.1888	0.2899	0.0795	0.174
Stage 12	$7.13 \times 10^{-5}$	0.1652	0.1351	0.1454	0.0125	0.180
Stage 13	$4.10 \times 10^{-5}$	0.1738	0.2207	0.1847	-0.0449	0.094
Stage 14	$6.22 \times 10^{-5}$	0.1754	0.1726	0.1496	-0.0063	0.169
Stage 15	$5.69 \times 10^{-5}$	0.2197	0.2106	0.1746	-0.0437	0.171
Stage 16	$5.66 \times 10^{-5}$	0.2350	0.2049	0.1741	-0.0380	0.165
Stage 17	$5.21 \times 10^{-5}$	0.2317	0.2005	0.1545	-0.0376	0.137
Stage 18	$7.42 \times 10^{-5}$	0.1970	0.1555	0.1362	-0.0003	0.207
Stage 19	$5.07 \times 10^{-5}$	0.1825	0.2152	0.1898	-0.0618	0.128
Stage 20	$4.81 \times 10^{-5}$	0.2052	0.2296	0.2707	-0.1172	0.120
Stage 21	$4.91 \times 10^{-5}$	0.2297	0.1945	0.2125	-0.1216	0.116
Stage 22	$5.20 \times 10^{-5}$	0.2000	0.1961	0.1705	-0.0307	0.140
Stage 23	$2.87 \times 10^{-5}$	0.1369	0.1367	0.0591	-0.0006	0.061
Stage 24	$2.83 \times 10^{-5}$	0.1694	0.0982	0.0386	0.0015	0.053
Stage 25	$3.16 \times 10^{-5}$	0.0050	0.1150	0.0560	0.0006	0.054

25. Since microcloth is the finest material to polish the sample surface, this last change point also naturally signals the endpoint of the polishing process. We therefore stop the process there.

What if we did not use the GP model parameter for decision making but rather used  $\bar{S}_a$  and relied on experience? Because the polishing process is a destructive process, it is impossible to repeat the same process on the same sample once it has already been polished. In Sec. 4.3, our team conducts another experiment largely based on experience. We can garner additional insight from this control-group experiment. Here, we can nevertheless take a retrospective look at the sequence of  $\bar{S}_a$  values in Table 2

and see if it offers strong enough clues for pad change and the endpoint.

The value of  $\bar{S}_a$  sees rapid declines in the initial few steps, but it is a bit difficult to decide when exactly to change to a finer grit pad. Too early a change could be detrimental; we will see such a misstep in the next experiment. After stage 5,  $\bar{S}_a$  fluctuates for a long stretch without a clear pattern to trigger pad change or the endpoint. Recall the switch to microcloth at stage 22 and is triggered by using the GP scale parameter and not by a pattern observed in  $\bar{S}_a$ .

**4.3 Polishing Based on Experience.** To contrast the polishing effectiveness with and without guidelines in Algorithm 1, we conduct a control-group experiment, referred to as experiment #2 here, which is largely based on experience. As in experiment #1, the same three grit sizes of pad are available to the team. The polishing process setting of experiment #2 is shown in Table 3. Experiment #2 comprises a total of 23 stages.

Although the control-group team does not use the GP parameters for their decision making, they nonetheless save all the data, which is later used to fit the GP model retrospectively for comparison purposes. The parameters, together with  $\bar{S}_a$ , are presented in Table 4.

In experiment #2, the control-group team switches the pad too soon, after observing the first significant decrease in  $\bar{S}_a$  at stage 3. This is after about 10-min operation using the coarsest pad, and this change is consistent with the typical rule on polishing time under this grit size.

But the use of 1200-grit pad at this point turns out to be a frustrating experience because it fails to remove certain surface anomalies after more than 280 min of operation. As a result,  $\bar{S}_a$  is stubbornly stuck at a high roughness level (above  $1 \mu\text{m}$ ). The team changes back to the 800-grit pad, and that action produces a noticeable improvement.

The next pad change takes place at stage 13, where the team changes the pad again to 1200-grit and uses it to polish the sample for 160 min. After that, the pad is changed to microcloth, which is used for the rest of the operation. All these changes are based on intuition rather than on quantitative measures because there is no clear pattern in  $\bar{S}_a$  to advise these actions.

Had the team used the scale parameter to advise pad change, the first change point would have been at stage 9. In fact, should the 800-grit pad have been applied without going back and forth between the 800-grit and 1200-grit pads, we believe that it would

**Table 3 The physical polishing process settings for experiment #2**

From	To	Time (min)	Down force (lbs)	Head speed (rpm)	Base speed (rpm)	Pad	Alumina solution
Stage 0	Stage 1	3	10	100	50	800	No
Stage 1	Stage 2	4	10	100	50	800	No
Stage 2	Stage 3	3	10	100	50	800	No
Stage 3	Stage 4	4	10	100	50	1200	No
Stage 4	Stage 5	30	10	100	50	1200	No
Stage 5	Stage 6	40	10	100	50	1200	No
Stage 6	Stage 7	90	10	100	50	1200	No
Stage 7	Stage 8	120	10	100	50	1200	No
Stage 8	Stage 9	10	10	100	50	800	No
Stage 9	Stage 10	15	10	100	50	800	No
Stage 10	Stage 11	30	10	100	50	800	No
Stage 11	Stage 12	60	10	100	50	800	No
Stage 12	Stage 13	70	10	100	50	800	No
Stage 13	Stage 14	160	5	100	50	1200	No
Stage 14	Stage 15	60	5	130	70	Microcloth	Yes
Stage 15	Stage 16	110	2	110	60	Microcloth	Yes
Stage 16	Stage 17	120	1	120	60	Microcloth	Yes
Stage 17	Stage 18	30	1	120	60	Microcloth	Yes
Stage 18	Stage 19	30	1	120	60	Microcloth	Yes
Stage 19	Stage 20	30	1	120	60	Microcloth	Yes
Stage 20	Stage 21	30	1	120	60	Microcloth	Yes
Stage 21	Stage 22	30	1	120	60	Microcloth	Yes

**Table 4 GP parameter estimates for experiment #2**

Stage	$\sigma_\epsilon$	$\theta_x$	$\theta_s$	$\sigma_\tau$	$\beta_0$	$\bar{S}a$
Stage 0	2.4835	0.1750	0.0767	46.7615	-1.7576	24.873
Stage 1	0.7358	0.1859	0.0786	16.4013	0.0475	4.422
Stage 2	1.3406	0.1919	0.0792	56.7901	-20.7301	5.452
Stage 3	1.0424	0.1753	0.0607	22.2674	-4.7154	1.582
Stage 4	0.4503	0.1908	0.0793	20.5310	-9.0351	1.403
Stage 5	0.4583	0.2067	0.0760	15.6656	-6.7286	1.363
Stage 6	0.8649	0.2006	0.0617	10.8910	-1.3232	1.556
Stage 7	0.4107	0.2034	0.0675	8.8720	-2.2710	1.188
Stage 8	0.2472	0.1960	0.0524	5.6581	-1.4584	0.740
Stage 9	0.2488	0.1636	0.0330	2.5462	-0.6953	0.109
Stage 10	0.3032	0.6312	0.0253	3.5086	-0.7442	0.069
Stage 11	0.0569	13.0682	0.0085	0.3262	0.0040	0.123
Stage 12	0.0466	2.2709	0.0189	1.1242	-0.2537	0.130
Stage 13	0.0407	4.7289	0.0393	5.8157	0.3392	0.104
Stage 14	0.0536	3.8895	0.0048	0.1158	-0.0073	0.031
Stage 15	0.1097	1.16E05	0.0045	0.1153	-0.0070	0.023
Stage 16	0.0748	2.93E05	0.0050	0.1035	-0.0074	0.028
Stage 17	0.0453	4.0675	0.0069	0.0859	-0.0020	0.028
Stage 18	0.0359	5.4172	0.0060	0.0931	-0.0003	0.026
Stage 19	0.0236	7.8204	0.0084	0.1309	-0.0031	0.023
Stage 20	0.0851	1.9713	0.0039	0.1624	-0.0103	0.027
Stage 21	0.0377	4.3438	0.0041	0.1265	-0.0054	0.026
Stage 22	0.0203	8.6444	0.0075	0.1188	-0.0031	0.026

not take nine stages to arrive at the change point. The second pad change point would have taken place at stage 12, and the final process would have stopped at stage 17, assuming that the scale parameter trend and pattern remain the same. Approximately 300 min would be saved if the process had been guided by the decision rule in Algorithm 1.

We would like to articulate two observations supporting our claim of the merit of using the GP-based guideline and the shortcoming of the experience-based decision process.

The first observation is made when visually comparing the surface quality at stage 3, stage 8, and stage 9 in Fig. 8. It is not difficult to understand why the change to the 1200-grit pad is premature, because there is still noticeable raw roughness left on the surface at stage 3. The application of the 1200-grit pad helps but is not effective, as evident by the same pattern of roughness still observable at stage 8. After applying the 800-grit pad again, it is apparent that the surface at stage 9 is much smoother and the raw roughness has been removed to a much greater extent. Therefore, it is more reasonable to switch to the 1200-grit pad after stage 9.

The second observation is about the significant change in  $\theta_x$  from stages 16 to 17, while  $\bar{S}a$  is fluctuating rather than showing a clear pattern. To us, that is a sign of over-polishing, signaling either a pad change or an endpoint of the process (if the finest pad is being used already). From stage 17 through stage 22, while the fluctuation message is confirmed by the plateau in both  $\theta_x$  and  $\bar{S}a$ , the scale parameter,  $\theta_s$ , is apparently more sensitive and can flag the endpoint sooner.

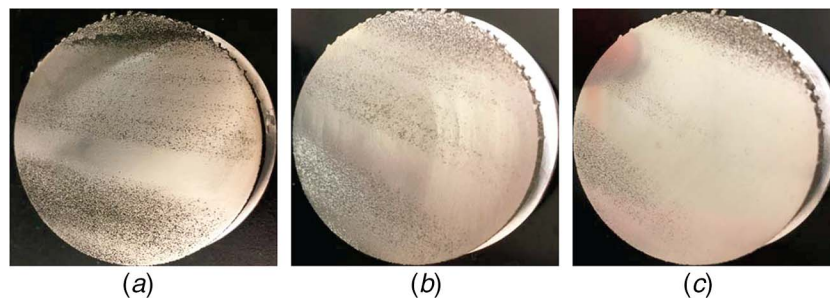


**Fig. 8 Sample surface quality at stage 3 to stage 8 and stage 9 in experiment #2: (a) stage 3, (b) stage 8, and (c) stage 9**

## 5 Simulation Experiment

Polishing is an abrasive operation. Once polished, the part cannot be restored to the original state to conduct a what-if study, such as “What if we change the pad at an earlier stage? What benefit could it bring?” To facilitate such studies, we decide to build a simulation model to mimic the polishing process. The simulation model attempts to capture the essence of the polishing operation, but considering all the complexities involved, in its current version it is not yet capable of precisely replicating the physical outcome. It does produce a sequence of parameter patterns mimicking what we observe in the physical experiments; for that, we deem it useful.

**5.1 Simulation Procedures.** The surface profile obtained from the actual unpolished surface is used as the initial sample surface to perform the simulation. Let us call this  $z_0(x, y)$ . The simulation of the polishing operation consists of two elements: first, modeling the abrasive profile associated with the polishing pad and second, modeling the action of applying a polishing pad to the sample surface.

**5.1.1 Polishing Pad Abrasiveness Generation.** To simulate the polishing pad, we first define the baseline denoted by  $\mu^{(t)}$  at stage  $t$  (see Fig. 9). Initially, this is set to the average surface roughness of the workpiece. Next, spherical abrasives with a fixed radius  $R$  and normally distributed height  $h$  (measured from the center) with mean  $\mu^{(t)}$  and standard deviation  $\sigma^{(t)}$  are generated. The inter asperity distance,  $a$ , is exponentially distributed with a scale parameter of  $5R$  and is determined based on the distribution of abrasives on the polishing pad as observed from the scanning electron micrographs.

In the  $(t + 1)$ th polishing stage, the baseline is lowered by one unit height, namely,  $1 \mu\text{m}$ . The new baseline is accordingly updated to  $\mu^{(t)} - 1$ . This is not to say that the material removed in the polishing at every stage is always of  $1 \mu\text{m}$  height. But the actual baseline height change is difficult to estimate. The use of a constant here is a simplification. We tried different values of constant and found that the final result is not sensitive to the choice, as long as the reduction in height is large enough.

**5.1.2 Polishing Process Simulation.** The polishing process simulation is implemented with the following three steps:

- (1) The first step involves intersection of the polishing pad with the workpiece surface (shown as the shaded area in Fig. 9). This is the amount of material removed in one pass. After  $t$  polishing passes, let the workpiece surface be denoted by  $z_t(x, y)$ .
- (2) Next, we superimpose the pad roughness ( $z_c(x, y)$ ) to the workpiece surface ( $z_t(x, y)$ ) obtained in the previous step. This is accomplished by taking the following three actions:
  - Generate the height profiles according to an uncorrelated Gaussian distribution, i.e.,  $z_u(x, y) \sim \mathcal{N}(0, 1)$ , where  $x$  and  $y$  are coordinates of the 2D surface,  $z_u$  is the height of roughness, and the subscript,  $u$ , indicates “uncorrelated.”

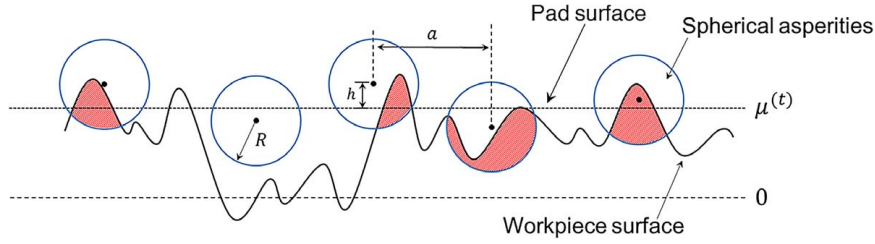


**Fig. 9 Schematic showing the modeling of abrasive profile and the convolution of the sample surface profile (heights  $z$ ) with the abrasive profile (with heights  $h$ ). The spherical asperities are assumed to be embedded on the pad surface. The material removed during a particular cut is the shaded area.**

- To obtain the Gaussian distributed height profile with exponential autocovariance, we perform the convolution of  $z_u(x, y)$  with an exponentially varying auto-covariance function given as

$$z_c(x, y) = \eta \int_{-\infty}^{\infty} \exp\left(-2 \frac{|x-x'| + |y-y'|}{l}\right) z_u(x', y') dx' dy'$$

where  $l$  is the scale length and  $\eta$  controls the amplitude of the surface  $z_c(x, y)$ . To determine  $\eta$ , it is reasonable to consider that the average surface roughness in the final stage of the polishing process is indicative of the pad roughness and is estimated by equating  $z_c(x, y)$  to the final stage surface roughness  $\bar{S}_a$  as

$$\eta = \bar{S}_a \left[ \int_{-\infty}^{\infty} \exp\left(-2 \frac{|x-x'| + |y-y'|}{l}\right) z_u(x', y') dx' dy' \right]^{-1}$$

The use of the exponential auto-covariance function is because such choice is well suited for mimicking the real pad roughness. As polishing ensues, the surface gets smoother and nearby locations are more and more similar to each other, thereby increasing the autocorrelation. However, the surface still contains sub-micrometer aberrations. In this regard, exponential autocovariance function is better suited to mimic the real pad roughness as compared to other auto-covariance functions such as squared exponential that results in ultra-smooth profiles. To numerically obtain the convolution, we use the convolution theorem that states that the Fourier transform  $\mathcal{F}$  of the convolution of two signals is the point-wise product of the Fourier transform of the two signals, i.e.,  $f * g = \mathcal{F}^{-1}\{\mathcal{F}(f) \cdot \mathcal{F}(g)\}$ , where  $*$  is the convolution operator,  $\cdot$  is the point-wise product, and  $\mathcal{F}^{-1}$  is the inverse Fourier transform.

- Then, we superimpose the pad roughness  $z_c(x, y)$  to the surface  $z_f(x, y)$  obtained after the first operation.
- (3) Finally, random white noise is added to account for un-modeled system noise and measurement noises.

In the following simulation experiment, polishing pads of dimension  $1024 \mu\text{m} \times 1024 \mu\text{m}$  are used with parameters specification elaborated in Sec. 5.2.

**5.2 Simulation Experiments.** We use the simulation to study the timing and impact of a single pad change action, presumably from a 800-grit pad to a 1200-grit pad.

In the first version of the simulation experiment, we guide the pad change purely by  $\bar{S}_a$ . The rule is: change the pad when  $\bar{S}_a$  is at or below  $0.1 \mu\text{m}$ . Following this rule, the pad change takes place after stage 7. Before and including stage 7, the pad parameters used are  $R = 1 \mu\text{m}$ ,  $\sigma^{(t)} = 0.1 \mu\text{m}$ , and  $l$  (in  $\mu\text{m}$ )  $\sim$  uniform(100,

**Table 5 A simulation experiment guided by  $\bar{S}_a$**

Stage	$\sigma_\epsilon$	$\theta_x$	$\theta_s$	$\sigma_\tau$	$\beta_0$	$\bar{S}_a$
Stage 1	2.4560	9.6238	$3.8 \times 10^{-2}$	4.7364	-0.5693	0.1705
Stage 2	2.4379	10.4220	$3.5 \times 10^{-2}$	4.5112	-0.5333	0.1552
Stage 3	2.4329	$5.00 \times 10^4$	$3.4 \times 10^{-5}$	4.1452	-0.5132	0.1411
Stage 4	2.4144	356.33	$2.5 \times 10^{-3}$	4.0056	-0.4662	0.1291
Stage 5	2.3985	527.99	$2.4 \times 10^{-3}$	3.8852	-0.4496	0.1180
Stage 6	2.3838	$2.43 \times 10^4$	$3.0 \times 10^{-4}$	3.7736	-0.4526	0.1090
Stage 7	2.3700	$1.20 \times 10^3$	$2.3 \times 10^{-3}$	3.6464	-0.4198	0.1007
Stage 8	2.3581	$1.74 \times 10^3$	$2.2 \times 10^{-3}$	3.5274	-0.4047	0.0933
Stage 9	2.3512	$2.52 \times 10^3$	$2.1 \times 10^{-3}$	3.4321	-0.3911	0.0689
Stage 10	2.3460	$2.98 \times 10^3$	$2.1 \times 10^{-3}$	3.3723	-0.3844	0.0653
Stage 11	2.3411	$3.53 \times 10^3$	$2.1 \times 10^{-3}$	3.3126	-0.3772	0.0623

**Table 6 The simulation experiment guided by  $\theta_x$**

Stage	$\sigma_\epsilon$	$\theta_x$	$\theta_s$	$\sigma_\tau$	$\beta_0$	$\bar{S}_a$
Stage 3	2.4329	$5.00 \times 10^4$	$3.4 \times 10^{-5}$	4.1452	-0.5132	0.1411
Stage 4	2.4144	356.33	$2.5 \times 10^{-3}$	4.0056	-0.4662	0.1291
Stage 5	2.4029	527.24	$2.5 \times 10^{-3}$	3.9086	-0.4505	0.1048
Stage 6	2.3878	919.14	$2.4 \times 10^{-3}$	3.7890	-0.4346	0.0936
Stage 7	2.3732	$1.19 \times 10^3$	$2.3 \times 10^{-3}$	3.6691	-0.4201	0.0855
Stage 8	2.3613	$1.73 \times 10^3$	$2.2 \times 10^{-3}$	3.5491	-0.4055	0.0760
Stage 9	2.3502	$2.52 \times 10^3$	$2.1 \times 10^{-3}$	3.4298	-0.3910	0.0691
Stage 10	2.3397	$3.58 \times 10^3$	$2.1 \times 10^{-3}$	3.3107	-0.3771	0.0623
Stage 11	2.3299	$4.86 \times 10^3$	$2.0 \times 10^{-3}$	3.1921	-0.3632	0.0567

Note: Stages 3 and 4 data are taken from Table 5. Stages 1 and 2 are omitted.

500). After stage 7, the pad parameters are changed to  $R = 0.5 \mu\text{m}$ ,  $\sigma^{(t)} = 0.01 \mu\text{m}$ , and  $l$  (in  $\mu\text{m}$ )  $\sim$  uniform(100, 500).

If we look at the value of  $\theta_x$ , we notice that following the rule in Algorithm 1, the pad change would have happened at stage 4, much sooner than using  $\bar{S}_a$ . Then, a relevant question is what would happen, had we indeed changed the pad after stage 4.

The simulation experiment allows us to rewind the process by using the simulation data saved in every step. Therefore, we basically go back to stage 4 and take the outcome of the simulated polishing up to that stage but apply a 1200-grit pad instead. The simulated outcome of the new process is presented in Table 6. In the old process (Table 5), the polishing action takes eight stages to reduce the surface roughness to 0.093, whereas in the new process (Table 6), the polishing action takes six stages to accomplish the same. By the eighth stage, the new process polishes the surface to the roughness level of 0.076, a further 18% reduction in roughness.

## 6 Concluding Remarks and Future Work

This work proposes a model-guided polishing process which alleviates the inconsistency in the decision process of surface

polishing and can potentially shorten the polishing time compared to the present practice. The essence of the model-guided decision process is using correlation parameters in GP models to reveal surface anomalies and to reflect potential over-polishing. While this work takes titanium alloy as samples in the polishing experiments to illustrate the judicious use of the GP models, the proposed modeling framework and GP-based decision protocol are applicable to a broad array of material polishing processes.

We take advantage of the surface recovery property in the simulation experiment to verify the *what-if* scenario. Moreover, the simulation experiment is a promising approach that may substitute the expensive physical polishing experiments, especially if more of the polishing complexities, e.g., the workpiece surface degradation, can be incorporated.

There are a number of other topics that are worth continuing attention. The first that comes to mind is the use of a constant,  $\alpha = 0.9$  or  $0.95$ , in our proposed decision process. While this empirical choice appears effective in our application, we speculate that a more adaptive change point detection procedure may be beneficial for shortening the polishing time and/or effecting a better polished surface. The second possibility is to explore whether the micro-scale correlation parameter,  $\theta_s$ , helps the

decision process. We do not use it in the proposed decision process but wonder if it is useful at all. The third possible extension is to compare the quantile curves at various locations on the surface and test the homogeneity among the curves. The homogeneity among the quantile curves could serve as a new metric for signaling pad change or the endpoint. If this idea works out, it is certainly interesting to see which of the metrics, the correlation parameters or the curve homogeneity test, is a better metric.

### Acknowledgment

The authors acknowledge the support from Army Research Lab (CRADA JWS 14-10-06; Funder ID: 10.13039/100006754), NSF (Grant No. IIS-1849085; Funder ID: 10.13039/501100008982), and Texas A&M Office (Funder ID: 10.13039/100007904) of President's X-grant Program.

### Appendix: Surface Images of the Additive Manufacturing Part Throughout the Polishing Process in Experiment #1

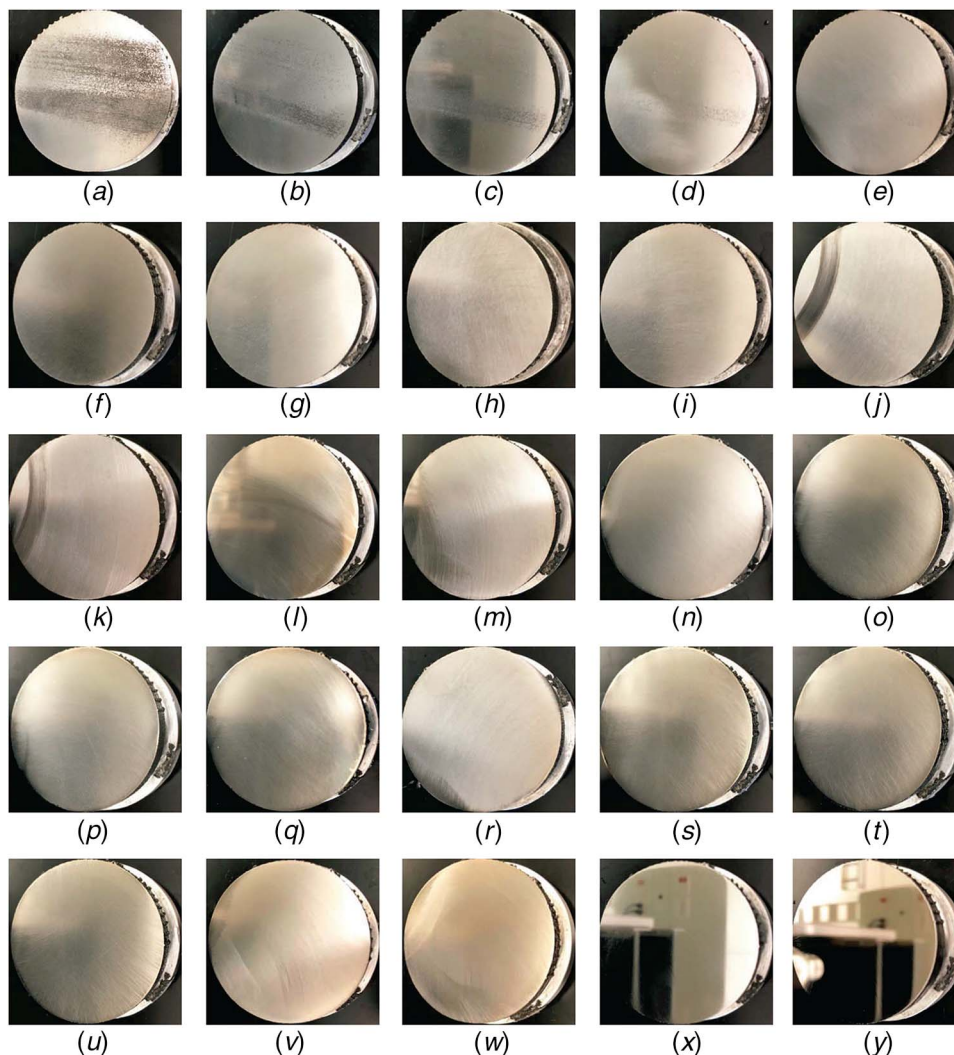


Fig. 10 Sample surface change from stage 1 through the endpoint: (a) stage 1, (b) stage 2, (c) stage 3, (d) stage 4, (e) stage 5, (f) stage 6, (g) stage 7, (h) stage 8, (i) stage 9, (j) stage 10, (k) stage 11, (l) stage 12, (m) stage 13, (n) stage 14, (o) stage 15, (p) stage 16, (q) stage 17, (r) stage 18, (s) stage 19, (t) stage 20, (u) stage 21, (v) stage 22, (w) stage 23, (x) stage 24, and (y) stage 25

## References

- [1] Frazier, W. E., 2014, "Metal Additive Manufacturing: A Review," *J. Mater. Eng. Perform.*, **23**(6), pp. 1917–1928.
- [2] Chan, K. S., Koike, M., Mason, R. L., and Okabe, T., 2013, "Fatigue Life of Titanium Alloys Fabricated by Additive Layer Manufacturing Techniques for Dental Implants," *Metal. Mater. Trans. A*, **44**(2), pp. 1010–1022.
- [3] Luo, J., and Dornfeld, D. A., 2001, "Material Removal Mechanism in Chemical Mechanical Polishing: Theory and Modeling," *IEEE Trans. Semicond. Manuf.*, **14**(2), pp. 112–133.
- [4] Zhou, C., Shan, L., Hight, J. R., Danyluk, S., Ng, S., and Paszkowski, A. J., 2002, "Influence of Colloidal Abrasive Size on Material Removal Rate and Surface Finish in  $\text{SiO}_2$  Chemical Mechanical Polishing," *Tribol. Trans.*, **45**(2), pp. 232–238.
- [5] Komanduri, R., Lucca, D., and Tani, Y., 1997, "Technological Advances in Fine Abrasive Processes," *CIRP Ann.*, **46**(2), pp. 545–596.
- [6] Wang, Z., Bukkapatnam, S. T., Kumara, S. R., Kong, Z., and Katz, Z., 2014, "Change Detection in Precision Manufacturing Processes Under Transient Conditions," *CIRP Ann.*, **63**(1), pp. 449–452.
- [7] Liu, J. P., Beyca, O. F., Rao, P. K., Kong, Z. J., and Bukkapatnam, S. T., 2017, "Dirichlet Process Gaussian Mixture Models for Real-Time Monitoring and Their Application to Chemical Mechanical Planarization," *IEEE Trans. Autom. Sci. Eng.*, **14**(1), pp. 208–221.
- [8] Bibby, T., and Holland, K., 1998, "Endpoint Detection for CMP," *J. Electron. Mater.*, **27**(10), pp. 1073–1081.
- [9] Helu, M., Chien, J., and Dornfeld, D., 2014, "In-Situ CMP Endpoint Detection Using Acoustic Emission," *Proc. CIRP*, **14**, pp. 454–459.
- [10] ISO 4287, 1997, *Geometrical Product Specifications (GPS), Surface Texture: Profile Method—Terms, Definitions and Surface Texture Parameters*, International Organization for Standardization, Geneva, Switzerland.
- [11] Bukkapatnam, S. T., Iquebal, A. S., and Kumara, S. R., 2018, "Planar Random Graph Representations of Spatiotemporal Surface Morphology: Application to Finishing of 3-d Printed Components," *CIRP Ann.*, **67**(1), pp. 495–498.
- [12] Cressie, N. A. C., 1991, *Statistics for Spatial Data*, John Wiley & Sons, New York.
- [13] Rasmussen, C. E., and Williams, C. K., 2006, *Gaussian Processes for Machine Learning*, The MIT Press, Cambridge, MA.
- [14] Moroni, G., Syam, W. P., and Petro, S., 2014, "Towards Early Estimation of Part Accuracy in Additive Manufacturing," *Proc. CIRP*, **21**, pp. 300–305.
- [15] Tapia, G., Elwany, A., and Sang, H., 2016, "Prediction of Porosity in Metal-Based Additive Manufacturing Using Spatial Gaussian Process Models," *Addit. Manuf.*, **12**, pp. 282–290.
- [16] Tapia, G., Khairallah, S., Matthews, M., King, W. E., and Elwany, A., 2018, "Gaussian Process-Based Surrogate Modeling Framework for Process Planning in Laser Powder-Bed Fusion Additive Manufacturing of 316L Stainless Steel," *Int. J. Adv. Manuf. Technol.*, **94**(9–12), pp. 3591–3603.
- [17] Iquebal, A. S., Sagapuram, D., and Bukkapatnam, S., 2016, "Surface Plastic Flow in Polishing of Rough Surfaces," *Scientific Reports*, **9**, Article No. 10617.
- [18] Stewart, M., 2000, "A New Approach to the Use of Bearing Area Curve," Society of Manufacturing Engineers, <http://numericalengineering.com/wp-content/uploads/2018/03/Training-A-New-Approach-to-the-Use-of-Bearing-Area-Curve-FC900229.pdf>, Accessed March 14, 2019.
- [19] Ramsay, J. O., and Dalzell, C., 1991, "Some Tools for Functional Data Analysis," *J. R. Stat. Soc. Ser. B (Methodol.)*, **53**(3), pp. 539–572.
- [20] Ramsay, J., and Silverman, B., 2005, *Functional Data Analysis*, Springer, New York.
- [21] Shi, J., Wang, B., Murray-Smith, R., and Titterton, D., 2007, "Gaussian Process Functional Regression Modeling for Batch Data," *Biometrics*, **63**(3), pp. 714–723.